

Transport in the non-Fermi liquid phase of isotropic Luttinger semimetals

Ipsita Mandal^{1,2} and Hermann Freire³

¹*Faculty of Science and Technology, University of Stavanger, 4036 Stavanger, Norway*

²*Institute of Nuclear Physics, Polish Academy of Sciences,
W. E. Radzikowskiego 152, PL-31342 Kraków, Poland*

³*Instituto de Física, Universidade Federal de Goiás, 74.001-970, Goiânia-GO, Brazil*

(Dated: June 19, 2022)

Luttinger semimetals have quadratic band crossings at the Brillouin zone-center in three spatial dimensions. Coulomb interactions in a model that describes these systems stabilize a non-trivial fixed point associated with a non-Fermi liquid state, also known as the Luttinger-Abrikosov-Beneslavskii phase. We calculate the optical conductivity $\sigma(\omega)$ and the dc conductivity $\sigma_{dc}(T)$ of this phase by means of the Kubo formula and the Mori-Zwanzig memory matrix method, respectively. Interestingly, we find that $\sigma(\omega)$, as a function of the frequency ω of an applied ac electric field, is characterized by a small violation of the hyperscaling property in the clean limit, which is in marked contrast to the low-energy effective theories that possess Dirac quasiparticles in the excitation spectrum and obey hyperscaling. Furthermore, the effects of weak short-ranged disorder on the temperature-dependence of $\sigma_{dc}(T)$ give rise to a much stronger power-law suppression at low temperatures compared to the clean limit. Our findings demonstrate that these disordered systems are actually power-law insulators. Our theoretical results agree qualitatively with the data from recent experiments performed on Luttinger semimetal compounds like the pyrochlore iridates [$(Y_{1-x}Pr_x)_2Ir_2O_7$].

Contents

I. Introduction

I. Introduction	1
II. Model	2
III. Current-current correlation function and optical conductivity	3
A. One-loop contribution	4
B. Two-loop contributions	4
C. Scaling of the optical conductivity up to two-loop order	4
IV. Memory matrix formalism	5
A. Current-momentum susceptibility at finite T	6
B. Memory matrix calculation	7
C. Scaling of dc conductivity	8
V. Summary and outlook	8
VI. Acknowledgments	9
References	9
A. d_a -function algebra	10
B. Two-Loop Contributions to the current-current correlators	11
1. Self-energy corrections	11
2. Vertex-like corrections	12
C. Two-loop contributions to the current-momentum susceptibility	12

Theories of non-Fermi liquid (NFL) phases in two and three-dimensions are one of the biggest enigmas in the field of strongly-correlated quantum matter and even today, after many decades of intense research, remain largely an unsolved problem. A deep understanding of these NFL phases turns out to be crucial in view of the fact that these states naturally lead to new emergent phases (such as high-temperature superconductivity, topological phenomena in semi-metals and superconductors, etc) as some external parameter like temperature, pressure or doping is varied in the system. It is a theoretically challenging task to study such systems, and consequently there have been intensive efforts dedicated to building a framework to understand them [1–18]. They are also referred to as critical Fermi surface states, as the breakdown of the Fermi liquid theory is brought about by the interplay between the soft fluctuations of the Fermi surface and some gapless bosonic fluctuations.

Recently, there has been also an upsurge of interest in a new frontier of this field where NFL phases can be observed at a Fermi point, i.e., in the absence of a large Fermi surface. From the analysis of the electronic structure of compounds like pyrochlore iridates, the half-Heusler compounds, and grey-Sn, a minimal effective model to describe such systems turns out to be the well-known three-dimensional Luttinger model with quadratic band crossings at the zone-center (i.e., the Γ point). Consequently, the materials that are well-described by this low-energy effective theory are nowadays known as “Luttinger semimetals” in the literature [19–24]. This novel class of materials not only exhibits strong spin-orbit coupling, but also

has strong electron-electron interactions. Since electron-electron interactions are not screened in these systems, an effective description must also include long-range Coulomb interactions. Interestingly, this problem was studied for the first time back in 1974 by Abrikosov [25], who demonstrated, using renormalization group (RG) arguments, that the Coulomb interaction in the model stabilizes a non-trivial fixed point associated with a new NFL state in three spatial dimensions, which was later called the Luttinger-Abrikosov-Beneslavskii (LAB) phase [19]. This fixed point is stable provided that time-reversal symmetry and the cubic symmetries are preserved in the system. This earlier work was later rediscovered and extended by Moon *et al.* [19], who calculated the universal power-law exponents describing various physical quantities in this LAB phase in the clean (i.e. disorder-free) limit, including the conductivity, susceptibility, specific heat, and the magnetic Gruneisen number.

From a strictly theoretical point of view, there has also been an increasing interest in the LAB phase, since it may realize the so-called “minimal-viscosity” scenario [26], in which the ratio of the shear viscosity η with the entropy s is close to the Kovtun-Son-Starinets ratio [27], i.e., $\eta/s \gtrsim 1/(4\pi)$. This means that these systems may be considered as a new example of a strongly-interacting “nearly-perfect fluid”. Other important examples that satisfy this condition include the hydrodynamical fluid that emerges in a clean single-layer graphene sheet at charge neutrality point [28], the quark-gluon plasma [29] generated in relativistic heavy-ion colliders, and ultracold fermionic gases tuned to the unitarity limit [30].

Naturally, transport properties of NFL phases are extremely important in order to characterize these systems. One of the widely used methods to calculate non-equilibrium properties is the application of the quantum Boltzmann equations. This method has many merits, and along with the well-established ε -expansion, it has been successfully used to discuss the hydrodynamical regime of many quantum critical systems. However, this approach also has some limitations, as one of its main assumptions is that the quasiparticle excitations exist even at low energies in the model, which is of course not valid at the LAB fixed point. Therefore, alternative methods to calculate transport properties, which do not rely on the existence of quasiparticles at low energies, should be used instead in order to provide an unbiased evaluation of such properties in NFL systems at low temperatures. For this reason, in the present work, we will apply the Kubo formula, and also its implementation using the Mori-Zwanzig memory matrix formalism, to the Luttinger model with long-range Coulomb interactions, in order to describe some transport coefficients of the LAB phase. More specifically, we will compute the optical conductivity $\sigma(\omega)$ at $T = 0$ as a function of the frequency ω of an applied ac electric field, and the dc resistivity $\rho(T)$ as a function of temperature T with the addition of weak short-ranged disorder. Since the ef-

fects of disorder are relevant in the renormalization group flow sense [20, 21] for the LAB phase, they turn out to be important also for the study of the transport properties of the system at low temperatures.

The main results obtained in the paper are the following: We find that $\sigma(\omega)$ in the LAB phase is characterized by a small violation of the hyperscaling property in the clean limit, in contrast to the low-energy effective theories that possess Dirac quasiparticles in the excitation spectrum and obey hyperscaling. Furthermore, on investigating the effects of weak short-ranged disorder on the dc conductivity $\sigma_{dc}(T)$, we find that $\sigma_{dc}(T)$ displays a much stronger power-law suppression at low temperatures compared to the corresponding result in the clean limit. We then compare this theoretical result with the available experimental data.

The paper is structured as follows. In Sec. II, we define the LAB phase for the Luttinger Hamiltonian coupled with long-range Coulomb interactions. Then, we calculate the optical conductivity of the LAB phase up to two-loop order in Sec. III, using the Kubo formula. Next, in Sec. IV, we calculate the dc resistivity of the model as a function of temperature, with the addition of weak short-ranged disorder using the memory matrix formalism. Finally, in Sec. V, we end with a summary and some outlook. Appendix A illustrates the derivation of some relations involving the $\ell = 2$ spherical harmonics in d spatial dimensions, that are useful for the loop integrals. The details of the two-loop calculations have been explained in Appendices B and C.

II. Model

To begin with, we consider the Luttinger model with quadratic band crossings at the zone-center in three spatial dimensions, where the low-energy bands form a four-dimensional representation of the lattice symmetry group [19]. The $\mathbf{k} \cdot \mathbf{p}$ Hamiltonian for the non-interacting system, in the absence of disorder, takes the following form [31]:

$$\mathcal{H}_0 = \sum_{a=1}^N d_a(\mathbf{k}) \Gamma_a + \frac{k^2}{2m'}, \quad d_a(\mathbf{k}) = \frac{\tilde{d}_a(\mathbf{k})}{2m}, \quad (1)$$

where the Γ_a matrices are the rank-four irreducible representations of the Clifford algebra relation $\{\Gamma_a, \Gamma_b\} = 2\delta_{ab}$ in the Euclidean space. We have used the common notation $\{A, B\} = AB + BA$ for denoting the anticommutator. There are five such matrices that are related to the familiar gamma matrices of the Dirac equation (plus the matrix conventionally denoted as Γ_5), but with the Euclidean metric $\{\Gamma_a, \Gamma_b\} = 2\delta_{ab}$ (instead of the Minkowski metric). In $d = 3$, the space of 4×4 Hermitian matrices is spanned by the identity matrix, the five 4×4 Gamma matrices Γ_a , and the ten distinct matrices $\Gamma_{ab} = \frac{1}{2i} [\Gamma_a, \Gamma_b]$. Furthermore, the $\tilde{d}_a(\mathbf{k})$'s are the $l = 2$ spherical harmonics that have the

following structure:

$$\begin{aligned} \tilde{d}_1(\mathbf{k}) &= \sqrt{3} k_y k_z, & \tilde{d}_2(\mathbf{k}) &= \sqrt{3} k_x k_z, & \tilde{d}_3(\mathbf{k}) &= \sqrt{3} k_x k_y, \\ \tilde{d}_4(\mathbf{k}) &= \frac{\sqrt{3} (k_x^2 - k_y^2)}{2}, & \tilde{d}_5(\mathbf{k}) &= \frac{2k_z^2 - k_x^2 - k_y^2}{2}. \end{aligned} \quad (2)$$

The isotropic $\frac{k^2}{2m'}$ term in Eq. (1) with no spinor structure makes the band mass of the conduction and valence bands unequal in the model.

We consider a setting with N_f independent flavors of fermions. The most general Euclidean action with these

properties may be written as

$$S_0 = \sum_{i=1}^{N_f} \int d\tau d^3\mathbf{x} \left\{ \psi_i^\dagger(\tau, \mathbf{x}) [\partial_\tau + \mathcal{H}_0 + i e \varphi(\tau, \mathbf{x})] \psi_i(\tau, \mathbf{x}) + \frac{c}{2} [\nabla \varphi(\tau, \mathbf{x})]^2 \right\}, \quad (3)$$

where the Coulomb interactions are mediated by a scalar boson field $\varphi(\mathbf{x})$ with no dynamics. If we integrate out the scalar boson to obtain the Coulomb interaction as an effective four-fermion term, this yields the total action

$$S = \sum_{i=1}^{N_f} \int \frac{d\omega d^3\mathbf{k}}{(2\pi)^4} \tilde{\psi}_i^\dagger(\omega, \mathbf{k}) (-i\omega + \mathcal{H}_0) \tilde{\psi}_i(\omega, \mathbf{k}) - \frac{e^2 \mu^{\varepsilon/2}}{2c} \sum_{i=1}^{N_f} \int \frac{d\omega d\omega' d\Omega d^3\mathbf{q} d^3\mathbf{k} d^3\mathbf{k}'}{(2\pi)^{12}} V(|\mathbf{q}|) \tilde{\psi}_i^\dagger(\omega, \mathbf{k}) \tilde{\psi}_i^\dagger(\omega', \mathbf{k}') \tilde{\psi}_i(\omega + \Omega, \mathbf{k} + \mathbf{q}) \tilde{\psi}_i(\omega' - \Omega, \mathbf{k}' - \mathbf{q}), \quad (4)$$

where the Coulomb interaction vertex is given by $V(|\mathbf{q}|) = \frac{1}{q^2}$ in the momentum space. The tilde over ψ indicates that it is the Fourier-transformed version. We have also included a mass scale μ such that $\frac{e^2}{c}$ is dimensionless.

The bare Green's function for each fermionic flavor is given by

$$G_0(\omega, \mathbf{k}) = \frac{i\omega - \frac{\mathbf{k}^2}{2m'} + \mathbf{d}(\mathbf{k}) \cdot \boldsymbol{\Gamma}}{-(i\omega - \frac{\mathbf{k}^2}{2m'})^2 + |\mathbf{d}(\mathbf{k})|^2}, \quad (5)$$

where $|\mathbf{d}(\mathbf{k})|^2 = \frac{\mathbf{k}^4}{4m'^2}$. On occasions, to lighten the notation, we will use $\mathbf{d}_{\mathbf{k}}$ to denote $\mathbf{d}(\mathbf{k})$. The non-trivial LAB fixed point [25] for the clean system is given by $e = e^*$, where

$$e^{*2} = \frac{60 \pi^2 c \varepsilon}{m (4 + 15 N_f)}. \quad (6)$$

The dynamical critical exponent z at this fixed point is given by $z^* = 2 - 4\varepsilon/(15N_f + 4)$, where $\varepsilon = 4 - d$, with d being the number of spatial dimensions.

The current \mathbf{J} and momentum \mathbf{P} operators of the Luttinger semimetal are given by:

$$\begin{aligned} \mathbf{J} &= \sum_i \int \frac{d^d\mathbf{k}}{(2\pi)^3} \tilde{\psi}_i^\dagger(\mathbf{k}) [\nabla_{\mathbf{k}} \mathbf{d}(\mathbf{k}) \cdot \boldsymbol{\Gamma}] \tilde{\psi}_i(\mathbf{k}), \\ \mathbf{P} &= \sum_i \int \frac{d^d\mathbf{k}}{(2\pi)^3} \mathbf{k} \tilde{\psi}_i^\dagger(\mathbf{k}) \tilde{\psi}_i(\mathbf{k}), \end{aligned} \quad (7)$$

which can be calculated using the Noether's theorem.

III. Current-current correlation function and optical conductivity

In this section, we will compute the optical conductivity $\sigma(\omega) = \sigma_{zz}(\omega, \mathbf{q} = \mathbf{0})$ at $T = 0$ via the Kubo formula

$$\sigma(\omega) = - \frac{\langle J_z J_z \rangle (i\Omega)}{\Omega} \Big|_{i\Omega \rightarrow \omega + i0^+}, \quad (8)$$

for current flowing along the z -direction. Since the model is isotropic, the scaling relation is not dependent on the choice of the direction of the current flow. We take an approach similar to the ones taken in the context of NFL models in the presence of a large Fermi surface [13, 15, 32].

We will employ the scheme developed by Moon *et al.* [19], where the radial momentum integrals are performed with respect to a $d = 4 - \varepsilon$ dimensional measure $\int \frac{|\mathbf{k}|^{3-\varepsilon} d|\mathbf{k}|}{(2\pi)^{4-\varepsilon}}$, but the $\boldsymbol{\Gamma}$ matrix structure is as in $d = 3$. The angular integrals are performed only over the three-dimensional sphere parameterized by the polar and azimuthal angles (θ, ϕ) . However, the overall angular integral of an isotropic function $\int_{\hat{\Omega}} \cdot 1$ is taken to be $2\pi^2$ (which is appropriate for the total solid angle in $d = 4$), and the angular integrals are normalized accordingly. Therefore, the angular integrations are performed with respect to the following measure:

$$\int dS(\dots) \equiv \frac{\pi}{2} \int_0^\pi d\theta \int_0^{2\pi} d\phi \sin\theta(\dots), \quad (9)$$

where the $\pi/2$ is inserted for the sake of normalization. To perform the full loop integrals, we will use the relations shown in Appendix A.

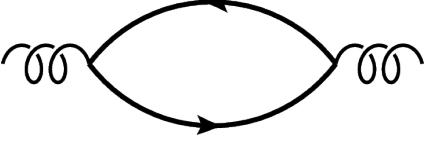


FIG. 1. Feynman diagram for the contribution to the current-current correlation function at one-loop order.

A. One-loop contribution

The current-current correlation function at one-loop level is given by a simple fermionic loop with two current insertions, as shown in Fig. 1. In the present model, it evaluates to

$$\begin{aligned}
\langle J_z J_z \rangle_{1\text{loop}}(i\omega) &= - \sum_{i=1}^{N_f} \int \frac{dk_0}{2\pi} \int \frac{d^3\mathbf{k}}{(2\pi)^3} \text{Tr} \left[\{ \partial_{k_z} \mathbf{d}(\mathbf{k}) \cdot \boldsymbol{\Gamma} \} G_0(k+q) \{ \partial_{k_z} \mathbf{d}(\mathbf{k}) \cdot \boldsymbol{\Gamma} \} G_0(k) \right] \\
&= -N_f \int \frac{dk_0}{2\pi} \int \frac{d^3\mathbf{k}}{(2\pi)^3} \text{Tr} \left[\{ \partial_{k_z} \mathbf{d}(\mathbf{k}) \cdot \boldsymbol{\Gamma} \} \frac{i k_0 + i\omega + \mathbf{d}(\mathbf{k}) \cdot \boldsymbol{\Gamma}}{-(i k_0 + i\omega)^2 + |\mathbf{d}(\mathbf{k})|^2} \{ \partial_{k_z} \mathbf{d}(\mathbf{k}) \cdot \boldsymbol{\Gamma} \} \frac{i k_0 + \mathbf{d}(\mathbf{k}) \cdot \boldsymbol{\Gamma}}{-(i k_0)^2 + |\mathbf{d}(\mathbf{k})|^2} \right] \\
&= -4 N_f \int \frac{dk_0}{2\pi} \int \frac{d^3\mathbf{k}}{(2\pi)^3} \frac{-\{ \partial_{k_z} \mathbf{d}(\mathbf{k}) \}^2 (k_0 + \omega) k_0 + \frac{1}{4} \{ \partial_{k_z} \mathbf{d}^2(\mathbf{k}) \}^2 - \{ \partial_{k_z} \mathbf{d}(\mathbf{k}) \}^2 \mathbf{d}^2(\mathbf{k})}{\left[-(i k_0 + i\omega)^2 + |\mathbf{d}(\mathbf{k})|^2 \right] \left[-(i k_0)^2 + |\mathbf{d}(\mathbf{k})|^2 \right]} \\
&= - \frac{N_f m^{1-\frac{\varepsilon}{2}} |\omega|^{2-\frac{\varepsilon}{2}}}{\pi^2 \varepsilon}, \tag{10}
\end{aligned}$$

where $q = (\omega, \mathbf{0})$. Consequently, at zeroth order, the optical conductivity $\sigma(\omega)$ is proportional to $\omega^{1-\frac{\varepsilon}{2}}$. In $d = 3$, this result then agrees with the so-called hyperscaling property, where the optical conductivity is expected to scale as $\sigma(\omega) \sim \omega^{(d-2)/z}$ for $\omega \gg T$ (the value of the critical exponent z is equal to 2 in the non-interacting limit).

In the next subsection, we will consider the effects of the Coulomb interaction, which will show how it affects the hyperscaling property of the model.

B. Two-loop contributions

Let us now consider the one-loop fermion self-energy corrections to the current-current correlator. We include a factor of 2, since the diagrams in Figs. 2(a) and 2(b) give equal contributions. This yields the result

$$\begin{aligned}
\langle J_z J_z \rangle_{2\text{loop}}^{(1)}(i\omega) &= \frac{e^2 N_f m^{2-\frac{\varepsilon}{2}} |\omega|^{2-\frac{\varepsilon}{2}} \left(\frac{\mu}{m|\omega|} \right)^{\varepsilon/2}}{90 \pi^4 c \varepsilon^2} \\
&\quad - \frac{e^2 N_f m^{2-\frac{\varepsilon}{2}} |\omega|^{2-\frac{\varepsilon}{2}} \ln \left(\frac{m|\omega|}{\mu} \right)}{180 \pi^4 c \varepsilon}. \tag{11}
\end{aligned}$$

The calculational details of the above equation can be found in Appendix B 1.

As for the diagram in Fig. 2(c), which refers to a vertex-like correction, it evaluates to

$$\begin{aligned}
\langle J_z J_z \rangle_{2\text{loop}}^{(2)}(i\omega) &= \frac{e^2 N_f m^{2-\frac{\varepsilon}{2}} |\omega|^{2-\frac{\varepsilon}{2}} \left(\frac{\mu}{m|\omega|} \right)^{\varepsilon/2}}{120 \pi^4 c \varepsilon^2} \\
&\quad - \frac{e^2 N_f m^{2-\frac{\varepsilon}{2}} |\omega|^{2-\frac{\varepsilon}{2}} \ln \left(\frac{m|\omega|}{\mu} \right)}{240 \pi^4 c \varepsilon}. \tag{12}
\end{aligned}$$

Again, the details of the latter calculation can be found in Appendix B 2.

C. Scaling of the optical conductivity up to two-loop order

In order to obtain the renormalized quantity in the effective field theory model, we have to use the fact that $\frac{1}{\varepsilon^2}$ terms are cancelled by the corresponding counterterms of the renormalized action [33]. We also use the value $\frac{m e^* 2}{\pi^2 c} = \frac{60 \varepsilon}{4+15 N_f}$ at the NFL fixed point. Gathering all the terms, the final expression for $\langle J_z J_z \rangle$ up to two-loop order takes the form:

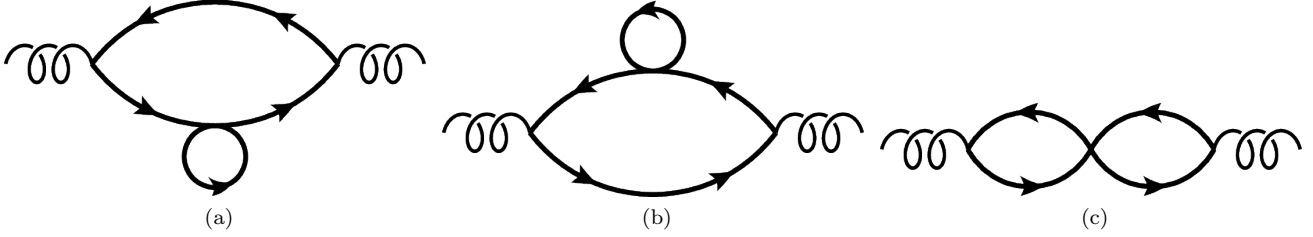


FIG. 2. Feynman diagrams for the contributions to the current-current correlation function at two-loop order.

$$\begin{aligned}
\langle J_z J_z \rangle(i\omega) &= \langle J_z J_z \rangle_{1\text{loop}}(i\omega) + \langle J_z J_z \rangle_{2\text{loop}}^{(1)}(i\omega) + \langle J_z J_z \rangle_{2\text{loop}}^{(2)}(i\omega) + \langle J_z J_z \rangle_{\text{counterterms}}^{(1)}(i\omega) \\
&= -\frac{N_f m^{1-\frac{\epsilon}{2}} |\omega|^{2-\frac{\epsilon}{2}}}{\pi^2 \epsilon} - \frac{e^{*2} N_f m^{2-\frac{\epsilon}{2}} |\omega|^{2-\frac{\epsilon}{2}} \ln\left(\frac{m|\omega|}{\mu}\right)}{180 \pi^4 c \epsilon} - \frac{e^{*2} N_f m^{2-\frac{\epsilon}{2}} |\omega|^{2-\frac{\epsilon}{2}} \ln\left(\frac{m|\omega|}{\mu}\right)}{240 \pi^4 c \epsilon} \\
&= -\frac{N_f m^{1-\frac{\epsilon}{2}} |\omega|^{2-\frac{\epsilon}{2}}}{\pi^2 \epsilon} \left[1 + \frac{7\epsilon}{12(4+15N_f)} \ln\left(\frac{m|\omega|}{\mu}\right) \right] \\
&\simeq -\frac{N_f m^{1-\frac{\epsilon}{2}} |\omega|^{2-\frac{\epsilon}{2} + \frac{7\epsilon}{12(4+15N_f)}}}{\pi^2 \epsilon} \left(\frac{m}{\mu}\right)^{\frac{7\epsilon}{12(4+15N_f)}}, \tag{13}
\end{aligned}$$

after re-exponentiating the correction term coming from the two-loop diagrams. Therefore, the corrected optical conductivity scales as $\omega^{1-\frac{\epsilon}{2} + \frac{7\epsilon}{12(4+15N_f)}}$ after including the leading order corrections. Since the optical conductivity no longer scales as $\omega^{(d-2)/z}$, there exists a small violation (proportional to ϵ) of the hyperscaling for the optical conductivity at the LAB fixed point. This should be contrasted with other effective theories that possess Dirac quasiparticles in the excitation spectrum and obey hyperscaling.

IV. Memory matrix formalism

The second method that we will use in this work to calculate transport properties is the Mori-Zwanzig memory matrix approach (see, for example, Refs. [34–47]). Here, we will be very concise in explaining the technicalities of this formalism, as more details can be found in the literature [46]. In this framework, the matrix of conductivities can be written as

$$\sigma(\omega, T) = \frac{\chi_{JP}^R(T)}{[M_{PP}(T) - i\omega \chi_{JP}^R(T)] [\chi_{JP}^R(T)]^{-1}}, \tag{14}$$

with $\chi_{JP}^R(T)$ being the static retarded susceptibility (which gives the overlap of the current and momentum in the model), and $M_{PP}(T)$ is the memory matrix. For transport

along the z -direction, $\chi_{JP}^R(T)$ is given by

$$\chi_{J_z P_z}(T) = \int_0^\beta d\tau \langle J_z(\tau) P_z(0) \rangle. \tag{15}$$

As for the memory matrix, to leading order, it is given by (again, for transport along the z -direction)

$$M_{P_z P_z}(T) = \int_0^\beta d\tau \left\langle \dot{P}_z^\dagger(0) \frac{i}{\omega - L_0} \dot{P}_z(i\tau) \right\rangle, \tag{16}$$

where L_0 is the non-interacting Liouville operator. Consequently, the dc conductivity (i.e. $\sigma_{dc}(T) \equiv \sigma(\omega \rightarrow 0, T)$) is given by

$$\sigma_{dc}(T) = \frac{\chi_{J_z P_z}^2(T)}{\lim_{\omega \rightarrow 0} \frac{\text{Im} G_{\dot{P}_z \dot{P}_z}^R(\omega, T)}{\omega}}, \tag{17}$$

where $G_{\dot{P}_z \dot{P}_z}^R(\omega, T) = \left\langle \dot{P}_z(\omega) \dot{P}_z(-\omega) \right\rangle_0$ is the corresponding retarded correlation function in the Matsubara formalism. The notation $\langle \dots \rangle_0$ indicates that the average is in a grand-canonical ensemble to be taken with the non-interacting Hamiltonian of the system.

Since we want to investigate the effects of weak disorder in the present model, we add an impurity term in the action that couples to the fermionic density as represented by the action

$$S_{imp} = \sum_i \int d\tau d^3\mathbf{x} W(\mathbf{x}) \psi_i^\dagger(\tau, \mathbf{x}) \psi_i(\tau, \mathbf{x}). \tag{18}$$

We consider a weak uncorrelated disorder following a Gaussian distribution: $\langle W(\mathbf{x}) \rangle_{avg} = 0$ and $\langle W(\mathbf{x}) W(\mathbf{x}') \rangle = W_0 \delta^3(\mathbf{x} - \mathbf{x}')$, where W_0 represents the average magnitude square of the random potential experienced by the fermionic field. Therefore, to leading order in the impurity coupling strength, we obtain the expression:

$$\lim_{\omega \rightarrow 0} \frac{\text{Im} G_{\hat{P}_z \hat{P}_z}^R(\omega, T)}{\omega} \approx \lim_{\omega \rightarrow 0} W_0 \int \frac{d^3 \mathbf{q}}{(2\pi)^3} \frac{\text{Im} \Pi_0^R(\mathbf{q}, \omega)}{\omega}, \quad (19)$$

where $\Pi_0^R(\mathbf{q}, \omega) = \Pi_0(\mathbf{q}, i\omega \rightarrow \omega + i0^+)$ is the corresponding retarded correlation function in the model, with the polarizability $\Pi_0(\mathbf{q}, i\omega)$ being given by:

$$\begin{aligned} & \Pi_0(\mathbf{q}, i\omega) \\ &= -T N_f \sum_{k_0} \int \frac{d^3 \mathbf{k}}{(2\pi)^3} k_z^2 \text{Tr} [G_0(\mathbf{k} + \mathbf{q}, i k_0 + i\omega) G_0(\mathbf{k}, i k_0)]. \end{aligned} \quad (20)$$

$$\begin{aligned} -\chi_{J_z P_z} / N_f &= \left(\frac{e^2}{2c} \right) T^2 \sum_{k_0, \ell_0} \int \frac{d^3 \mathbf{k} d^3 \ell}{(2\pi)^6} k_z \text{Tr} \left[(\partial_{k_z} \mathbf{d}(\mathbf{k}) \cdot \boldsymbol{\Gamma}) G_0(k_0, \mathbf{k}) \frac{G_0(\ell_0, \mathbf{k} + \ell)}{\ell^2} G_0(k_0, \mathbf{k}) G_0(k_0, \mathbf{k}) \right] \\ &= \left(\frac{e^2}{2c} \right) T^2 \sum_{k_0, \ell_0} \int \frac{d^3 \mathbf{k} d^3 \ell}{(2\pi)^6} k_z \frac{\text{Tr} \left[(\partial_{k_z} \mathbf{d}(\mathbf{k}) \cdot \boldsymbol{\Gamma}) \frac{i k_0 + \mathbf{d}(\mathbf{k}) \cdot \boldsymbol{\Gamma}}{(i k_0)^2 - |\mathbf{d}(\mathbf{k})|^2} \frac{\mathbf{d}(\mathbf{k}) \cdot \boldsymbol{\Gamma}}{(i \ell_0)^2 - |\mathbf{d}(\mathbf{k})|^2} \frac{i k_0 + \mathbf{d}(\mathbf{k}) \cdot \boldsymbol{\Gamma}}{(i k_0)^2 - |\mathbf{d}(\mathbf{k})|^2} \frac{i k_0 + \mathbf{d}(\mathbf{k}) \cdot \boldsymbol{\Gamma}}{(i k_0)^2 - |\mathbf{d}(\mathbf{k})|^2} \right]}{(\mathbf{k} + \ell)^2} \\ &= 0, \end{aligned} \quad (21)$$

which also vanishes, as it also contains only odd powers of k_0 in the numerator after performing the trace in the above integral. One can verify that the same result holds for the two-loop diagram with vertex-like correction similar to Fig. 2(c). In fact, this vanishing result holds for all higher-order loops. This is related to the charge-conjugation (C) symmetry of the model, which is present for equal band masses. Since \mathbf{J} and \mathbf{P} are odd and even, respectively, under the C-symmetry, their overlap (i.e., the

We now proceed to calculate $\chi_{J_z P_z}(T)$ and $M_{P_z P_z}(T)$ in the static limit at finite temperatures in the following subsections. Note that, unlike in the previous section, instead of performing a systematic ε -expansion, we will work directly in $d = 3$ to overcome technical complexity. Furthermore, we will use a hard ultraviolet (UV) cutoff Λ for the momentum integrals, rather than using a dimensional regularization.

A. Current-momentum susceptibility at finite T

First we note that for equal band masses, implemented by taking the limit $m' \rightarrow \infty$, the current-momentum susceptibility clearly vanishes at one-loop order, as only an odd power of k_0 appears in the numerator. Furthermore, at two-loop order, the contribution to the current-momentum susceptibility due to self-energy insertions (similar to the diagrams depicted in Figs. 2(a) and 2(b)) is given by

current-momentum susceptibility) must be zero at all loop orders.

The vanishing of $\chi_{J_z P_z}(T)$ no longer holds for finite m' (i.e., for unequal conduction and valence band masses). For this reason, we will analyze the effect of higher-order corrections of the current-momentum susceptibility for finite m' .

We first calculate the free fermion susceptibility. It evaluates to

$$\begin{aligned} \chi_{J_z P_z}^{1loop}(T) &= -\lim_{\mathbf{q} \rightarrow 0} T N_f \sum_{k_0} \int \frac{d^3 \mathbf{k}}{(2\pi)^3} k_z \text{Tr} [(\partial_{k_z} \mathbf{d}(\mathbf{k}) \cdot \boldsymbol{\Gamma}) G_0(k_0, \mathbf{k} + \mathbf{q}) G_0(k_0, \mathbf{k})] \\ &= -4 T N_f \lim_{\mathbf{q} \rightarrow 0} \sum_{k_0} \int \frac{d^3 \mathbf{k}}{(2\pi)^3} k_z \frac{\left(i k_0 - \frac{(\mathbf{k} + \mathbf{q})^2}{2m'} \right) \frac{k_z k^2}{2m^2} + i k_0 \partial_{k_z} \mathbf{d}(\mathbf{k}) \cdot \mathbf{d}(\mathbf{k} + \mathbf{q})}{\left[\left(i k_0 + i\omega - \frac{(\mathbf{k} + \mathbf{q})^2}{2m'} \right)^2 - |\mathbf{d}_{\mathbf{k} + \mathbf{q}}|^2 \right] \left[\left(i k_0 - \frac{k^2}{2m'} \right)^2 - |\mathbf{d}_{\mathbf{k}}|^2 \right]}. \end{aligned} \quad (22)$$

We then perform the above summation over the fermionic

Matsubara frequency k_0 using the method of residues using

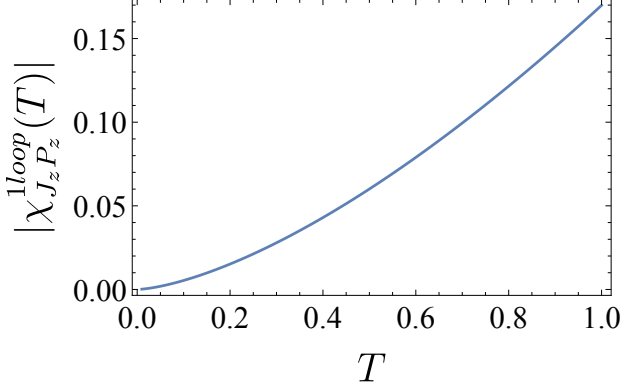


FIG. 3. Plot of the current-momentum susceptibility $\chi_{J_z P_z}^{1loop}(T)$ at one-loop order versus temperature T . Here, we have chosen the parameters $m = 1$, $m' = 5$, $N_f = 1$, and the UV cutoff Λ for the momentum integrals has been taken to the infinity limit (note that this result does not depend on the UV cutoff). The temperature dependence of this one-loop contribution is found to be $|\chi_{J_z P_z}^{1loop}(T)| \sim 0.170 T^{3/2}$.

the standard formula

$$T \sum_{\omega_n} h(\omega_n) = \sum_{z_k} \text{Res} [n_F(z) h(-iz)] \Big|_{z_k = \text{Poles of } h(-iz)}, \quad (23)$$

where $\text{Res}[\dots]$ denotes the residue, and $n_F(z) = \frac{1}{e^{z/T} + 1}$ is the Fermi-Dirac distribution function. Next we solve Eq. (22) by means of both analytical and numerical techniques using the software **Mathematica**, and obtain that $\chi_{J_z P_z}^{1loop}(T) \sim T^{3/2}$ (see Fig. 3).

One can easily check that there are only three Feynman diagrams at two-loop order. The corresponding diagrams are similar to the ones in Figs. 2(a), 2(b), and 2(c). These contributions evaluate to $\chi_{J_z P_z}^{2loop}(T) = \chi_{J_z P_z}^{(2,1)}(T) + \chi_{J_z P_z}^{(2,2)}(T)$, where

$$\chi_{J_z P_z}^{(2,1)}(T) \sim \left(\frac{8 e^2 \Lambda}{15 \pi^2 c T} \right) N_f T \sum_{k_0} \int \frac{d^3 \mathbf{k}}{(2\pi)^3} k_z \frac{\left[\left(i k_0 - \frac{\mathbf{k}^2}{2m'} \right)^3 (\partial_{k_z} \mathbf{d}_{\mathbf{k}} \cdot \mathbf{d}_{\mathbf{k}}) + 3 \left(i k_0 - \frac{\mathbf{k}^2}{2m'} \right) (\partial_{k_z} \mathbf{d}_{\mathbf{k}} \cdot \mathbf{d}_{\mathbf{k}}) |\mathbf{d}_{\mathbf{k}}|^2 \right]}{\left[\left(i k_0 - \frac{\mathbf{k}^2}{2m'} \right)^2 - |\mathbf{d}_{\mathbf{k}}|^2 \right]^3}, \quad (24)$$

$$\chi_{J_z P_z}^{(2,2)}(T) \sim \left(\frac{e^2 \Lambda}{2 \pi^2 c T} \right) N_f T \sum_{k_0} \int \frac{d^3 \mathbf{k}}{(2\pi)^3} k_z \frac{\left(i k_0 - \frac{\mathbf{k}^2}{2m'} \right) (\partial_{k_z} \mathbf{d}_{\mathbf{k}} \cdot \mathbf{d}_{\mathbf{k}})}{\left[\left(i k_0 - \frac{\mathbf{k}^2}{2m'} \right)^2 - |\mathbf{d}_{\mathbf{k}}|^2 \right]^2}. \quad (25)$$

We provide the detailed steps of the calculation in Appendix C. Finally, we evaluate the expressions in Eqs. (24) and (25) numerically, and obtain that $\chi_{J_z P_z}^{2loop}(T) \sim \frac{e^2}{c} T^{1/2}$ (see Fig. 4).

B. Memory matrix calculation

We now compute the Feynman diagram associated with the calculation of the memory matrix to leading order, as shown in Fig. 5, which is given by:

$$\begin{aligned} M_{P_z P_z}^{(0)}(T) &= -W_0 N_f \lim_{\omega \rightarrow 0} \frac{\text{Im} \left[\int \frac{d^3 \mathbf{k} d^3 \mathbf{q}}{(2\pi)^6} k_z^2 T \sum_{k_0} \text{Tr} [G_0(\omega + k_0, \mathbf{k} + \mathbf{q}) G_0(k_0, \mathbf{k})] \right]}{\omega} \Big|_{i\omega \rightarrow \omega + i\delta} \\ &= -4 W_0 N_f \lim_{\omega \rightarrow 0} \frac{\text{Im} \left[\int \frac{d^3 \mathbf{k} d^3 \mathbf{q}'}{(2\pi)^6} k_z^2 T \sum_{k_0} \frac{\left\{ i k_0 + i\omega - \frac{(\mathbf{k} + \mathbf{q})^2}{2m'} \right\} \left(i k_0 - \frac{\mathbf{k}^2}{2m'} \right) + (\mathbf{d}_{\mathbf{k} + \mathbf{q}} \cdot \mathbf{d}_{\mathbf{k}})}{\left\{ \left(i k_0 - \frac{(\mathbf{k} + \mathbf{q})^2}{2m'} \right)^2 - |\mathbf{d}_{\mathbf{k} + \mathbf{q}}|^2 \right\} \left\{ \left(i k_0 - \frac{\mathbf{k}^2}{2m'} \right)^2 - |\mathbf{d}_{\mathbf{k}}|^2 \right\}} \right]}{\omega} \Big|_{i\omega \rightarrow \omega + i\delta}. \quad (26) \end{aligned}$$

As before, the summation over k_0 is evaluated using the

method of residues. After performing the analytical contin-

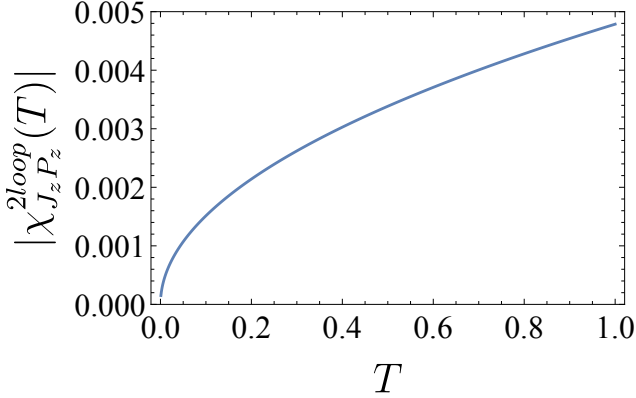


FIG. 4. Plot of the current-momentum susceptibility $\chi_{J_z P_z}^{2loop}(T)$ at two-loop order versus temperature T . Here, we have chosen the parameters $m = 1$, $m' = 5$, $e = 0.1$, $c = 1$, $N_f = 1$, and $\Lambda = 150$. The temperature dependence of this two-loop contribution is found to be $|\chi_{J_z P_z}^{(2loop)}(T)| \sim 0.005 T^{1/2}$.

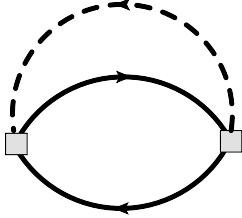


FIG. 5. Feynman diagram for the calculation of the leading-order contribution $M_{P_z P_z}^{(0)}(T)$ to the memory matrix. The solid line represents the bare fermionic propagator, whereas the dashed line represents the impurity line that carries only internal momentum and external energy ω .

uation, the resulting integral is then evaluated numerically which finally gives $M_{P_z P_z}^{(0)}(T)/W_0 \sim a' + b'/T$ (see Fig. 6), where a' and b' ($b' \gg a'$) are non-universal constants that depend only on the UV cutoff Λ . These constants are such that a' scales as Λ^2 and b' scales as Λ^4 , leading to $\frac{a'}{b'} \rightarrow 0$ for $\Lambda \rightarrow \infty$. Therefore, the final expression can be effectively approximated as $M_{P_z P_z}^{(0)}(T) \approx b'/T$ at low temperatures.

C. Scaling of dc conductivity

Taking into account all contributions, the scaling of the dc conductivity of the LAB phase in the presence of weak short-ranged scalar disorder is given by:

$$\sigma_{dc}(T) \equiv \frac{1}{\rho(T)} = \frac{|\chi_{J_z P_z}(T)|^2}{M_{P_z P_z}(T)} \sim T^n, \text{ where } 2 \leq n \leq 4, \quad (27)$$

and $\rho(T)$ is the resistivity. It is important to compare this expression with the dc conductivity of the LAB phase in

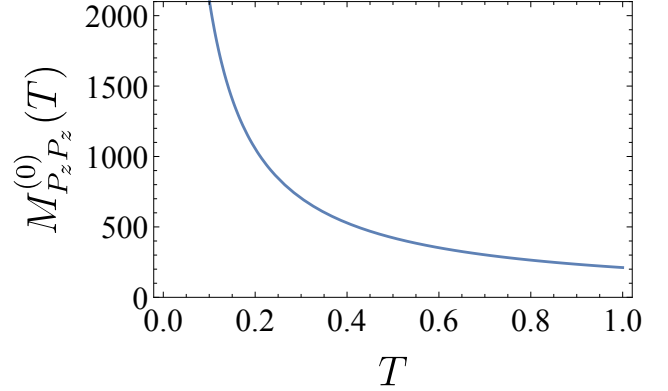


FIG. 6. Plot of $M_{P_z P_z}^{(0)}(T)$ versus temperature T . Here, we have chosen the parameters $W_0 = 1$, $N_f = 1$, $m = 1$, $m' = 5$, and $\Lambda = 150$. To obtain the memory matrix, we have performed the analytical continuation $i\omega \rightarrow \omega + i\delta$, where we have set $\delta = 10^{-9}$. The curve corresponds to the fit given by $g(T) = a' + b'/T$, where the parameters $a' \approx 0.059$ and $b' \approx 211.25$ depend only on the UV cutoff Λ .

the clean limit, which is given by $\sigma_{dc}(T) \sim T^{1/z^*}$ [19], where $z^* \approx 1.79$ is the renormalized dynamic critical exponent at the LAB fixed point for $d = 3$ and $N_f = 1$. This implies that $\sigma_{dc}(T)$ in the presence of disorder displays a much stronger power-law suppression as a function of temperature, which is an expected feature since the influence of disorder is a relevant perturbation in the vicinity of the LAB fixed point [20, 21]. It is also interesting to compare our theoretical results with recent transport experiments [48] performed on Luttinger semimetal compounds like pyrochlore iridates $[(Y_{1-x}Pr_x)_2Ir_2O_7]$. In these compounds, some degree of disorder is always present, and the dc resistivity has been found to follow the power-law $\rho(T) \sim T^{-n}$, with the exponent being $n \approx 2.98$ at zero doping. Therefore, we conclude that our present calculation is in qualitative agreement with these data.

V. Summary and outlook

In the present work, we have computed the scaling behavior of the optical conductivity and the dc conductivity of the LAB phase of Luttinger semimetals, by means of the Kubo formula and the Mori-Zwanzig memory matrix method, respectively. We have found that the optical conductivity in the LAB phase is characterized by a small violation (proportional to $\varepsilon = 4 - d$) of the hyperscaling property in the clean limit, in contrast to the low-energy effective theories that possess Dirac quasiparticles in the excitation spectrum (which obey hyperscaling). In the computations for dc conductivity $\sigma_{dc}(T)$, we have included the effects of weak short-ranged scalar disorder. We have shown that $\sigma_{dc}(T)$ exhibits a much stronger power-law suppression at low temperatures compared to the corresponding

result in the clean limit. This was an expected feature since the influence of disorder is a relevant perturbation in the system. Lastly, we have directly compared our theoretical prediction with recent experiments performed in disordered Luttinger semimetal materials like the pyrochlore iridates [48] and found qualitative agreement with the experimental data.

Finally, we would like to point out that it would be extremely interesting to investigate the effects of magnetic field on the magnetoresistance and the Hall coefficient of the LAB phase and compare the results with the corresponding experimental data available for the pyrochlore

iridates [48]. The magnetic field breaks time-reversal symmetry and, in view of this, it must be a strongly relevant perturbation that ultimately makes the LAB fixed point unstable at low energy scales. We leave this analysis for future studies.

VI. Acknowledgments

HF acknowledges funding from CNPq under Grant No. 310710/2018-9.

-
- [1] C. Nayak and F. Wilczek, “Renormalization group approach to low temperature properties of a non-Fermi liquid metal,” *Nuclear Physics B* **430**, 534–562 (1994).
- [2] C. Nayak and F. Wilczek, “Non-Fermi liquid fixed point in $2 + 1$ dimensions,” *Nuclear Physics B* **417**, 359–373 (1994).
- [3] M. J. Lawler, D. G. Barci, V. Fernández, E. Fradkin, and L. Oxman, “Nonperturbative behavior of the quantum phase transition to a nematic Fermi fluid,” *Phys. Rev. B* **73**, 085101 (2006).
- [4] David F. Mross, John McGreevy, Hong Liu, and T. Senthil, “Controlled expansion for certain non-fermi-liquid metals,” *Phys. Rev. B* **82**, 045121 (2010).
- [5] H.-C. Jiang, M. S. Block, R. V. Mishmash, J. R. Garrison, D. N. Sheng, O. I. Motrunich, and M. P. A. Fisher, “Non-Fermi-liquid d-wave metal phase of strongly interacting electrons,” *Nature (London)* **493**, 39–44 (2013).
- [6] Suk Bum Chung, Ipsita Mandal, Srinivas Raghu, and Sudip Chakravarty, “Higher angular momentum pairing from transverse gauge interactions,” *Phys. Rev. B* **88**, 045127 (2013).
- [7] Zhiqiang Wang, Ipsita Mandal, Suk Bum Chung, and Sudip Chakravarty, “Pairing in half-filled Landau level,” *Annals of Physics* **351**, 727 – 738 (2014).
- [8] Shouvik Sur and Sung-Sik Lee, “Chiral non-fermi liquids,” *Phys. Rev. B* **90**, 045121 (2014).
- [9] Denis Dalidovich and Sung-Sik Lee, “Perturbative non-fermi liquids from dimensional regularization,” *Phys. Rev. B* **88**, 245106 (2013).
- [10] Shouvik Sur and Sung-Sik Lee, “Quasilocal strange metal,” *Phys. Rev. B* **91**, 125136 (2015).
- [11] Ipsita Mandal and Sung-Sik Lee, “Ultraviolet/infrared mixing in non-fermi liquids,” *Phys. Rev. B* **92**, 035141 (2015).
- [12] Ipsita Mandal, “UV/IR Mixing In Non-Fermi Liquids: Higher-Loop Corrections In Different Energy Ranges,” *Eur. Phys. J. B* **89**, 278 (2016).
- [13] Andreas Eberlein, Ipsita Mandal, and Subir Sachdev, “Hyperscaling violation at the Ising-nematic quantum critical point in two-dimensional metals,” *Phys. Rev. B* **94**, 045133 (2016).
- [14] Ipsita Mandal, “Superconducting instability in non-fermi liquids,” *Phys. Rev. B* **94**, 115138 (2016).
- [15] Ipsita Mandal, “Scaling behaviour and superconducting instability in anisotropic non-fermi liquids,” *Annals of Physics* **376**, 89 – 107 (2017).
- [16] Sung-Sik Lee, “Recent developments in non-fermi liquid theory,” *Annual Review of Condensed Matter Physics* **9**, 227–244 (2018).
- [17] Dimitri Pimenov, Ipsita Mandal, Francesco Piazza, and Matthias Punk, “Non-fermi liquid at the f₁₁₀ quantum critical point,” *Phys. Rev. B* **98**, 024510 (2018).
- [18] Ipsita Mandal, “Critical fermi surfaces in generic dimensions arising from transverse gauge field interactions,” *Phys. Rev. Research* **2**, 043277 (2020).
- [19] Eun-Gook Moon, Cenke Xu, Yong Baek Kim, and Leon Balents, “Non-fermi-liquid and topological states with strong spin-orbit coupling,” *Phys. Rev. Lett.* **111**, 206401 (2013).
- [20] Rahul M. Nandkishore and S. A. Parameswaran, “Disorder-driven destruction of a non-fermi liquid semimetal studied by renormalization group analysis,” *Phys. Rev. B* **95**, 205106 (2017).
- [21] Ipsita Mandal and Rahul M. Nandkishore, “Interplay of Coulomb interactions and disorder in three-dimensional quadratic band crossings without time-reversal symmetry and with unequal masses for conduction and valence bands,” *Phys. Rev. B* **97**, 125121 (2018).
- [22] Ipsita Mandal, “Fate of superconductivity in three-dimensional disordered Luttinger semimetals,” *Annals of Physics* **392**, 179 – 195 (2018).
- [23] Ipsita Mandal, “Search for plasmons in isotropic Luttinger semimetals,” *Annals of Physics* **406**, 173–185 (2019).
- [24] Ipsita Mandal, “Tunneling in fermi systems with quadratic band crossing points,” *Annals of Physics* **419**, 168235 (2020).
- [25] A. A. Abrikosov, “Calculation of critical indices for zero-gap semiconductors,” *Sov. Phys.-JETP* **39**, 709 (1974).
- [26] Julia M. Link and Igor F. Herbut, “Hydrodynamic transport in the Luttinger-Abrikosov-Beneslavskii non-fermi liquid,” *Phys. Rev. B* **101**, 125128 (2020).
- [27] P. K. Kovtun, D. T. Son, and A. O. Starinets, “Viscosity in strongly interacting quantum field theories from black hole physics,” *Phys. Rev. Lett.* **94**, 111601 (2005).
- [28] Lars Fritz, Jörg Schmalian, Markus Müller, and Subir Sachdev, “Quantum critical transport in clean graphene,” *Phys. Rev. B* **78**, 085416 (2008).
- [29] G. Policastro, D. T. Son, and A. O. Starinets, “Shear viscosity of strongly coupled $n=4$ supersymmetric Yang-Mills plasma,” *Phys. Rev. Lett.* **87**, 081601 (2001).
- [30] C. Cao, E. Elliott, J. Joseph, H. Wu, J. Petricka, T. Schäfer, and J. E. Thomas, “Universal quantum viscosity in a uni-

- tary fermi gas,” *Science* **331**, 58–61 (2011).
- [31] Igor Boettcher and Igor F. Herbut, “Superconducting quantum criticality in three-dimensional luttinger semimetals,” *Phys. Rev. B* **93**, 205138 (2016).
- [32] Aavishkar A. Patel, Philipp Strack, and Subir Sachdev, “Hyperscaling at the spin density wave quantum critical point in two-dimensional metals,” *Phys. Rev. B* **92**, 165105 (2015).
- [33] Michael E. Peskin and Daniel V. Schroeder, *An Introduction to Quantum Field Theory* (Addison-Wesley, Reading, 1995).
- [34] Dieter Forster, *Hydrodynamic Fluctuations, Broken Symmetry, and Correlation Functions* (W. A. Benjamin, Reading, 1975).
- [35] A. Rosch and N. Andrei, “Conductivity of a Clean One-Dimensional Wire,” *Phys. Rev. Lett.* **85**, 1092–1095 (2000).
- [36] Raghu Mahajan, Maissam Barkeshli, and Sean A. Hartnoll, “Non-fermi liquids and the wiedemann-franz law,” *Phys. Rev. B* **88**, 125107 (2013).
- [37] Hermann Freire, “Controlled calculation of the thermal conductivity for a spinon Fermi surface coupled to a U(1) gauge field,” *Ann. Phys. (N. Y.)* **349**, 357–365 (2014).
- [38] Aavishkar A. Patel and Subir Sachdev, “dc resistivity at the onset of spin density wave order in two-dimensional metals,” *Phys. Rev. B* **90**, 165146 (2014).
- [39] Sean A. Hartnoll, Raghu Mahajan, Matthias Punk, and Subir Sachdev, “Transport near the ising-nematic quantum critical point of metals in two dimensions,” *Phys. Rev. B* **89**, 155130 (2014).
- [40] Jan Zaanen, Yan Liu, Ya-Wen Sun, and Koenraad Schalm, *Holographic Duality in Condensed Matter Physics* (Cambridge University Press, Cambridge, 2015).
- [41] Hermann Freire, “Memory matrix theory of the dc resistivity of a disordered antiferromagnetic metal with an effective composite operator,” *Ann. Phys. (N. Y.)* **384**, 142–154 (2017).
- [42] Hermann Freire, “Calculation of the magnetotransport for a spin-density-wave quantum critical theory in the presence of weak disorder,” *EPL (Europhysics Letters)* **118**, 57003 (2017).
- [43] Sean A. Hartnoll, Andrew Lucas, and Subir Sachdev, *Holographic Quantum Matter* (MIT Press, Cambridge, 2018).
- [44] Hermann Freire, “Thermal and thermoelectric transport coefficients for a two-dimensional SDW metal with weak disorder: A memory matrix calculation,” *EPL (Europhysics Letters)* **124**, 27003 (2018).
- [45] Xiaoyu Wang and Erez Berg, “Scattering mechanisms and electrical transport near an Ising nematic quantum critical point,” *Phys. Rev. B* **99**, 235136 (2019).
- [46] Lucas E. Vieira, Vanuildo S. de Carvalho, and Hermann Freire, “Dc resistivity near a nematic quantum critical point: Effects of weak disorder and acoustic phonons,” *Annals of Physics* **419**, 168230 (2020).
- [47] Xiaoyu Wang and Erez Berg, “Low frequency raman response near ising-nematic quantum critical point: a memory matrix approach,” (2020), [arXiv:2011.01818](https://arxiv.org/abs/2011.01818) [cond-mat.str-el].
- [48] Harish Kumar, K. C. Kharkwal, Kranti Kumar, K. Asokan, A. Banerjee, and A. K. Pramanik, “Magnetic and transport properties of the pyrochlore iridates $(\text{Y}_{1-x}\text{Pr}_x)_2\text{Ir}_2\text{O}_7$: Role of f - d exchange interaction and d - p orbital hybridization,” *Phys. Rev. B* **101**, 064405 (2020).

A. d_a -function algebra

We derive a set of useful relations [31] for the vector functions $\mathbf{d}(\mathbf{k})$ (whose components $d_a(\mathbf{k})$ are the $\ell = 2$ spherical harmonics in d spatial dimensions) and the generalized real $d \times d$ Gell-Mann matrices Λ_a ($a = 1, 2, \dots, d$). The matrices Λ_a are symmetric, traceless, and orthogonal, satisfying

$$\text{Tr}[\Lambda^a \Lambda^b] = 2 \delta_{ab}, \quad \sum_{a=1}^N (\Lambda^a)_{ij} (\Lambda^a)_{i'j'} = \delta_{il} \delta_{jj'} + \delta_{ij'} \delta_{jl} - \frac{2}{d} \delta_{ij} \delta_{l'j'}. \quad (\text{A1})$$

Hence, the index a (or b) runs from 1 to $N = \frac{(d-1)(d+2)}{2}$. We define the components of $\mathbf{d}(\mathbf{k})$ by

$$d_a(\mathbf{k}) = \sqrt{\frac{d}{2(d-1)}} \sum_{i,j=1}^d \frac{k_i (\Lambda^a)_{ij} k_j}{2m}. \quad (\text{A2})$$

This gives the following identities:

$$\begin{aligned}
\partial_{k_z} d_a(\mathbf{k}) &= \sqrt{\frac{d}{2(d-1)}} \frac{\sum_{j=1}^d (\Lambda^a)_{zj} k_j + \sum_{i=1}^d k_i (\Lambda^a)_{iz}}{2m} = \sqrt{\frac{2d}{d-1}} \frac{\sum_{j=1}^d (\Lambda^a)_{zj} k_j}{2m}, \\
\sum_{a=1}^N \{\partial_{k_z} d_a(\mathbf{k})\}^2 &= \frac{2d}{d-1} \sum_i^d \frac{(\delta_{ii} + \delta_{iz} \delta_{zi} - \frac{2}{d} \delta_{iz} \delta_{iz}) k_i^2}{4m^2} = \frac{d \times (\mathbf{k}^2 + \frac{d-2}{d} k_z^2)}{2m^2(d-1)}, \\
\sum_{a=1}^N d_a(\mathbf{k}) d_a(\mathbf{p}) &= \frac{d(\mathbf{k} \cdot \mathbf{p})^2 - \mathbf{k}^2 \mathbf{p}^2}{4m^2(d-1)}, \quad \sum_{a=1}^N [\partial_{k_z} d_a(\mathbf{k})] d_a(\mathbf{p}) = \frac{k_z \{d(\mathbf{k} \cdot \mathbf{p}) - \mathbf{p}^2\}}{2m^2(d-1)}, \\
\sum_{a=1}^N [\partial_{p_z} d_a(\mathbf{p})] [\partial_{k_z} d_a(\mathbf{k})] &= \sum_{a=1}^N \frac{2d}{4m^2(d-1)} \sum_{j=1}^d (\Lambda^a)_{zj} p_j \sum_{j'=1}^d (\Lambda^a)_{zj'} k_{j'} = \frac{d\mathbf{p} \cdot \mathbf{k} + (d-2) p_z k_z}{2m^2(d-1)}. \tag{A3}
\end{aligned}$$

For the special case of $\mathbf{p} = \mathbf{k}$, we obtain:

$$\sum_{a=1}^N d_a^2(\mathbf{k}) = \frac{\mathbf{k}^4}{4m^2}, \quad \frac{1}{2} \partial_{k_z} \sum_{a=1}^N d_a^2(\mathbf{k}) = \frac{k_z \mathbf{k}^2}{2m^2}. \tag{A4}$$

B. Two-Loop Contributions to the current-current correlators

1. Self-energy corrections

The diagrams in Figs. 2(a) and 2(b) involve inserting the one-loop fermion self-energy (Σ_1) corrections into the current-current correlator. We include a factor of 2 as the two diagrams give equal contributions and the expression incorporating this correction takes the form

$$\langle J_z J_z \rangle_{2\text{loop}}^{(1)}(i\omega) = -2 \sum_{i=1}^{N_f} \int \frac{dk_0}{2\pi} \int \frac{d^d \mathbf{k}}{(2\pi)^d} \text{Tr} [\{\partial_{k_z} \mathbf{d}(\mathbf{k}) \cdot \Gamma\} G_0(k+q) \Sigma_1(k+q) G_0(k+q) \{\partial_{k_z} \mathbf{d}(\mathbf{k}) \cdot \Gamma\} G_0(k)], \tag{B1}$$

where $\Sigma_1(\ell) = -\frac{m e^2}{15 \pi^2 c} \left(\frac{\mu^{1/2}}{|\ell|}\right)^\varepsilon \frac{\mathbf{d}(\ell) \cdot \Gamma}{\varepsilon}$ (see Ref. [20, 21]). This gives us:

$$\langle J_z J_z \rangle_{2\text{loop}}^{(1)}(i\omega) = \frac{2 N_f m e^2}{15 \pi^2 c \varepsilon} \int \frac{dk_0}{2\pi} \int \frac{d^d \mathbf{k}}{(2\pi)^d} \left(\frac{\mu^{1/2}}{|\mathbf{k}|}\right)^\varepsilon \frac{\text{term}_1}{\{k_0^2 + |\mathbf{d}(\mathbf{k})|^2\}^2 \{(k_0 + \omega)^2 + |\mathbf{d}(\mathbf{k})|^2\}}, \tag{B2}$$

where

$$\begin{aligned}
\text{term}_1 &= \text{Tr} [\{\partial_{k_z} \mathbf{d}(\mathbf{k}) \cdot \Gamma\} \{i k_0 + \mathbf{d}(\mathbf{k}) \cdot \Gamma\} \{\mathbf{d}(\mathbf{k}) \cdot \Gamma\} \{i k_0 + \mathbf{d}(\mathbf{k}) \cdot \Gamma\} \{\partial_{k_z} \mathbf{d}(\mathbf{k}) \cdot \Gamma\} \{i k_0 + i\omega + \mathbf{d}(\mathbf{k}) \cdot \Gamma\}] \\
&= -k_0^2 \text{Tr} [\{\partial_{k_z} \mathbf{d}(\mathbf{k}) \cdot \Gamma\} \{\mathbf{d}(\mathbf{k}) \cdot \Gamma\} \{\partial_{k_z} \mathbf{d}(\mathbf{k}) \cdot \Gamma\} \{\mathbf{d}(\mathbf{k}) \cdot \Gamma\}] \\
&\quad - 2 k_0 (k_0 + \omega) \text{Tr} [\{\partial_{k_z} \mathbf{d}(\mathbf{k}) \cdot \Gamma\} \{\mathbf{d}(\mathbf{k}) \cdot \Gamma\} \{\mathbf{d}(\mathbf{k}) \cdot \Gamma\} \{\partial_{k_z} \mathbf{d}(\mathbf{k}) \cdot \Gamma\}] \\
&\quad + \text{Tr} [\{\partial_{k_z} \mathbf{d}(\mathbf{k}) \cdot \Gamma\} \{\mathbf{d}(\mathbf{k}) \cdot \Gamma\} \{\mathbf{d}(\mathbf{k}) \cdot \Gamma\} \{\mathbf{d}(\mathbf{k}) \cdot \Gamma\} \{\partial_{k_z} \mathbf{d}(\mathbf{k}) \cdot \Gamma\} \{\mathbf{d}(\mathbf{k}) \cdot \Gamma\}] \\
&= -4 k_0^2 \left[2 \{\partial_{k_z} \mathbf{d}(\mathbf{k}) \cdot \mathbf{d}(\mathbf{k})\}^2 - \{\partial_{k_z} \mathbf{d}(\mathbf{k}) \cdot \partial_{k_z} \mathbf{d}(\mathbf{k})\} |\mathbf{d}(\mathbf{k})|^2 \right] - 8 k_0 (k_0 + \omega) \{\partial_{k_z} \mathbf{d}(\mathbf{k}) \cdot \partial_{k_z} \mathbf{d}(\mathbf{k})\} |\mathbf{d}(\mathbf{k})|^2 \\
&\quad + 8 \{\partial_{k_z} \mathbf{d}(\mathbf{k}) \cdot \mathbf{d}(\mathbf{k})\}^2 |\mathbf{d}(\mathbf{k})|^2 - 4 \{\partial_{k_z} \mathbf{d}(\mathbf{k}) \cdot \partial_{k_z} \mathbf{d}(\mathbf{k})\} |\mathbf{d}(\mathbf{k})|^4 \\
&= k_0^2 \mathbf{k}^6 \times \frac{(6-5d) \sin^2 \theta - d}{2(d-1) m^4} - k_0 \omega \mathbf{k}^6 \times \frac{d + (d-2) \sin^2 \theta}{(d-1) m^4} + \frac{\mathbf{k}^{10} [(3d-2) \sin^2 \theta - d]}{8(d-1) m^6}, \tag{B3}
\end{aligned}$$

using the identities from Appendix A.

Performing the integrals, we finally get:

$$\langle J_z J_z \rangle_{2\text{loop}}^{(1)}(i\omega) = \frac{e^2 N_f m^{2-\frac{\varepsilon}{2}} |\omega|^{2-\frac{\varepsilon}{2}}}{90 \pi^4 c \varepsilon^2} \left(\frac{\mu}{m\omega}\right)^{\varepsilon/2} - \frac{e^2 N_f m^{2-\frac{\varepsilon}{2}} |\omega|^{2-\frac{\varepsilon}{2}} \ln\left(\frac{m|\omega|}{\mu}\right)}{180 \pi^4 c \varepsilon}. \tag{B4}$$

2. Vertex-like corrections

The diagram in Fig. 2(c) equals $\langle J_z J_z \rangle_{2\text{loop}}^{(2)}(i\omega)$, where

$$\begin{aligned} & \frac{\langle J_z J_z \rangle_{2\text{loop}}^{(2)}(i\omega)}{\frac{e^2 \mu^{\varepsilon/2}}{2c}} \\ &= \sum_{i=1}^{N_f} \int \frac{dk_0 d\ell_0}{(2\pi)^2} \int \frac{d^d \mathbf{k} d^d \boldsymbol{\ell}}{(2\pi)^{2d}} \text{Tr} \left[\{ \partial_{k_z} \mathbf{d}(\mathbf{k}) \cdot \boldsymbol{\Gamma} \} G_0(k+q) \frac{1}{\ell^2} G_0(k+q+\ell) \{ \partial_{k_z+\ell_z} \mathbf{d}(\mathbf{k}+\boldsymbol{\ell}) \cdot \boldsymbol{\Gamma} \} G_0(k+\ell) G_0(k) \right] \\ &= \sum_{i=1}^{N_f} \int \frac{dk_0 d\ell_0}{(2\pi)^2} \int \frac{d^d \mathbf{k} d^d \boldsymbol{\ell}}{(2\pi)^{2d}} \text{Tr} \left[\{ \partial_{k_z} \mathbf{d}(\mathbf{k}) \cdot \boldsymbol{\Gamma} \} G_0(k_0+\omega, \mathbf{k}) \frac{1}{\ell^2} G_0(\ell_0+\omega, \mathbf{k}+\boldsymbol{\ell}) \{ \partial_{k_z+\ell_z} \mathbf{d}(\mathbf{k}+\boldsymbol{\ell}) \cdot \boldsymbol{\Gamma} \} G_0(\ell_0, \mathbf{k}+\boldsymbol{\ell}) G_0(k_0, \mathbf{k}) \right]. \end{aligned} \quad (\text{B5})$$

with $\ell = (\ell_0, \boldsymbol{\ell})$, We observe that the expression to be evaluated is

$$\frac{\langle J_z J_z \rangle_{2\text{loop}}^{(2)}(i\omega)}{\frac{e^2 \mu^{\varepsilon/2}}{2c}} = N_f \int \frac{d^d \mathbf{k} d^d \boldsymbol{\ell}}{(2\pi)^{2d}} \text{Tr} \left[\frac{\int \frac{dk_0}{2\pi} G_0(k_0-\omega, \mathbf{k}) \{ \partial_{k_z} \mathbf{d}(\mathbf{k}) \cdot \boldsymbol{\Gamma} \} G_0(k_0, \mathbf{k}) \int \frac{d\ell_0}{2\pi} G_0(\ell_0+\omega, \boldsymbol{\ell}) \{ \partial_{\ell_z} \mathbf{d}(\boldsymbol{\ell}) \cdot \boldsymbol{\Gamma} \} G_0(\ell_0, \boldsymbol{\ell})}{(\mathbf{k}+\boldsymbol{\ell})^2} \right], \quad (\text{B6})$$

after some clever regrouping of the terms in the integrand. Evaluating

$$\begin{aligned} & \int \frac{d\ell_0}{2\pi} G_0(\ell_0+\omega, \boldsymbol{\ell}) \{ \partial_{\ell_z} \mathbf{d}(\boldsymbol{\ell}) \cdot \boldsymbol{\Gamma} \} G_0(\ell_0, \boldsymbol{\ell}) = \int \frac{d\ell_0}{2\pi} \frac{-\ell_0(\ell_0+\omega) \partial_{\ell_z} \mathbf{d}(\boldsymbol{\ell}) \cdot \boldsymbol{\Gamma} + \frac{i(2\ell_0+\omega)\ell_z \ell^2}{2m^2} + \frac{\mathbf{d}(\boldsymbol{\ell}) \cdot \boldsymbol{\Gamma} \ell_z \ell^2}{2m^2}}{\{(\ell_0+\omega)^2 + |\mathbf{d}(\boldsymbol{\ell})|^2\} \{ \ell_0^2 + |\mathbf{d}(\boldsymbol{\ell})|^2 \}} \\ &= \frac{[2\ell_z \mathbf{d}(\boldsymbol{\ell}) - \ell^2 \partial_{\ell_z} \mathbf{d}(\boldsymbol{\ell})] \cdot \boldsymbol{\Gamma}}{2m \left(\frac{\ell^4}{m^2} + \omega^2 \right)}, \end{aligned} \quad (\text{B7})$$

we get:

$$\begin{aligned} & \frac{\langle J_z J_z \rangle_{2\text{loop}}^{(2)}(i\omega)}{\frac{e^2 \mu^{\varepsilon/2} N_f}{2c}} = \int \frac{d^d \mathbf{k} d^d \boldsymbol{\ell}}{(2\pi)^{2d}} \text{Tr} \left[\frac{[2k_z \{ \mathbf{d}(\mathbf{k}) \cdot \boldsymbol{\Gamma} \} - \mathbf{k}^2 \{ \partial_{k_z} \mathbf{d}(\mathbf{k}) \cdot \boldsymbol{\Gamma} \}] [2\ell_z \{ \mathbf{d}(\boldsymbol{\ell}) \cdot \boldsymbol{\Gamma} \} - \ell^2 \{ \partial_{\ell_z} \mathbf{d}(\boldsymbol{\ell}) \cdot \boldsymbol{\Gamma} \}]}{4m^2 (\mathbf{k}+\boldsymbol{\ell})^2 \left(\frac{\mathbf{k}^4}{m^2} + \omega^2 \right) \left(\frac{\ell^4}{m^2} + \omega^2 \right)} \right] \\ &= \int \frac{d^d \mathbf{k} d^d \boldsymbol{\ell}}{(2\pi)^{2d}} \frac{k_z \ell_z \left\{ d(\mathbf{k} \cdot \boldsymbol{\ell})^2 - \mathbf{k}^2 \ell^2 \right\} - 2k_z \ell_z \mathbf{k}^2 \{ d(\mathbf{k} \cdot \boldsymbol{\ell}) - \ell^2 \} + \mathbf{k}^2 \ell^2 \frac{d\mathbf{k} \cdot \boldsymbol{\ell} + (d-2)k_z \ell_z}{2}}{m^4 (d-1) (\mathbf{k}+\boldsymbol{\ell})^2 \left(\frac{\mathbf{k}^4}{m^2} + \omega^2 \right) \left(\frac{\ell^4}{m^2} + \omega^2 \right)}, \end{aligned} \quad (\text{B8})$$

using the identities from Appendix A. Performing the integrals, we finally obtain:

$$\langle J_z J_z \rangle_{2\text{loop}}^{(2)}(i\omega) = \frac{e^2 N_f m^{2-\frac{\varepsilon}{2}} |\omega|^{2-\frac{\varepsilon}{2}} \left(\frac{\mu}{m|\omega|} \right)^{\varepsilon/2}}{120 \pi^4 c \varepsilon^2} - \frac{e^2 N_f m^{2-\frac{\varepsilon}{2}} |\omega|^{2-\frac{\varepsilon}{2}} \ln \left(\frac{m|\omega|}{\mu} \right)}{240 \pi^4 c \varepsilon}. \quad (\text{B9})$$

C. Two-loop contributions to the current-momentum susceptibility

For the contributions at two-loop order represented by diagrams with self-energy insertions (similar to the diagrams in Figs. 2(a) and 2(b)), we get the expression:

$$\chi_{J_z P_z}^{(2,1)}(T) = -2T N_f \sum_{k_0} \int \frac{d^3 \mathbf{k}}{(2\pi)^3} k_z \text{Tr} [\{ \partial_{k_z} \mathbf{d}(\mathbf{k}) \cdot \boldsymbol{\Gamma} \} G_0(k_0, \mathbf{k}) \Sigma_T(k_0, \mathbf{k}) G_0(k_0, \mathbf{k}) G_0(k_0, \mathbf{k})], \quad (\text{C1})$$

where

$$\Sigma_T(k_0, \mathbf{k}) = -\frac{e^2}{c} T \sum_{\ell_0} \int \frac{d^3 \boldsymbol{\ell}}{(2\pi)^3} \frac{G_0(k_0+\ell_0, \mathbf{k}+\boldsymbol{\ell})}{\ell^2} = -\frac{e^2}{15\pi^2 c} \left[\frac{\Lambda}{T} \{ \mathbf{d}(\mathbf{k}) \cdot \boldsymbol{\Gamma} \} - \frac{5m}{4\Lambda_{IR}} |\mathbf{d}(\mathbf{k})| \right], \quad (\text{C2})$$

where Λ and Λ_{IR} correspond to the ultraviolet and infrared cutoff scales, respectively. In order to obtain the leading-order scaling in T of $\chi_{J_z P_z}^{(2,1)}(T)$, we can neglect the temperature independent term in Eq. (C2). Performing the trace in Eq. (C1), we obtain:

$$\chi_{J_z P_z}^{(1)}(T)/N_f \sim \left(\frac{2e^2 \Lambda}{15\pi^2 c T} \right) T \sum_{k_0} \int \frac{d^3 \mathbf{k}}{(2\pi)^3} k_z \frac{4 \left(i k_0 - \frac{\mathbf{k}^2}{2m'} \right)^3 (\partial_{k_z} \mathbf{d}_{\mathbf{k}} \cdot \mathbf{d}_{\mathbf{k}}) + 12 \left(i k_0 - \frac{\mathbf{k}^2}{2m'} \right) (\partial_{k_z} \mathbf{d}_{\mathbf{k}} \cdot \mathbf{d}_{\mathbf{k}}) |\mathbf{d}_{\mathbf{k}}|^2}{\left[\left(i k_0 - \frac{\mathbf{k}^2}{2m'} \right)^2 - |\mathbf{d}_{\mathbf{k}}|^2 \right]^3}. \quad (\text{C3})$$

For the two-loop diagram with vertex-like corrections (similar to Fig. 2(c)), we get the expression:

$$\chi_{J_z P_z}^{(2,2)}(T) = -T N_f \sum_{k_0} \int \frac{d^3 \mathbf{k}}{(2\pi)^3} k_z \text{Tr} \left[\{ \partial_{k_z} \mathbf{d}(\mathbf{k}) \cdot \mathbf{\Gamma} \} G_0(k_0, \mathbf{k}) \tilde{\Gamma}_1(k_0, \mathbf{k}) G_0(k_0, \mathbf{k}) \right], \quad (\text{C4})$$

where

$$\tilde{\Gamma}_1(k_0, \mathbf{k}) = -\frac{2e^2}{c} T \sum_{\ell_0} \int \frac{d^3 \ell}{(2\pi)^3} \frac{G_0(k_0 + \ell_0, \mathbf{k} + \ell) G_0(k_0 + \ell_0, \mathbf{k} + \ell)}{\ell^2} = -\frac{e^2}{16\pi^2 c T} \left(\Lambda + \frac{2m}{3\Lambda_{IR}} |\mathbf{d}(\mathbf{k})| \right). \quad (\text{C5})$$

Plugging this in, we get:

$$\chi_{J_z P_z}^{(2,2)}(T)/N_f = \left(\frac{e^2}{16\pi^2 c T} \right) T \sum_{k_0} \int \frac{d^3 \mathbf{k}}{(2\pi)^3} k_z \left(\Lambda + \frac{2m}{3\Lambda_{IR}} |\mathbf{d}(\mathbf{k})| \right) \frac{8 \left(i k_0 - \frac{\mathbf{k}^2}{2m'} \right) (\partial_{k_z} \mathbf{d}_{\mathbf{k}} \cdot \mathbf{d}_{\mathbf{k}})}{\left[\left(i k_0 - \frac{\mathbf{k}^2}{2m'} \right)^2 - |\mathbf{d}_{\mathbf{k}}|^2 \right]^2}. \quad (\text{C6})$$

In order to obtain the leading-order dependence on T , we can neglect the second term in Eq (C5).

In Fig. 4, we show the numerical result for $\chi_{J_z P_z}^{2loop}(T) = \chi_{J_z P_z}^{(2,1)}(T) + \chi_{J_z P_z}^{(2,2)}(T)$ as a function of temperature.
